ACS APPLIED MATERIALS & INTERFACES

Letter

www.acsami.org

Controlling Polarity of Organic Bulk Heterojunction Field-Effect Transistors via Solvent Additives

Jin Kuen Park,[†] Bright Walker,*[,‡] and Jung Hwa Seo*[,§]

[†]Department of Chemistry, Northwestern University, Evanston, Illinois 60208, United States

[‡]Interdisciplinary School of Green Energy, Ulsan National Institute of Science and Technology, Ulsan 689-798, Republic of Korea

[§]Department of Materials Physics, Dong-A University, Busan 604-714, Republic of Korea

Supporting Information

ABSTRACT: The effect of additives such as 1,8-diiodooctane (DIO) and 1-chloronaphthalene (CN) on the electronic structures, charge transport and phase separation of small-molecule-based bulk heterojunction (BHJ) films was investigated. Charge transport properties of the BHJ layers significantly changed via the introduction of additives, even though the molecular energy levels remained unchanged. X-ray photoelectron microscopy (XPM) images show the distribution of each phase of the blend films upon the use of additives. The CN additive, in particular, results in a well-percolated network through the active layer.

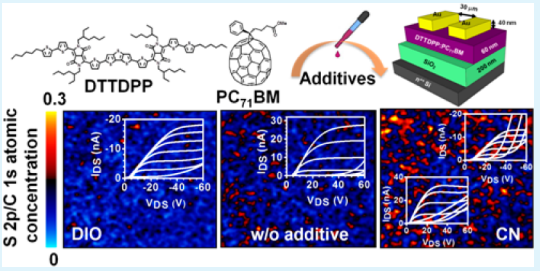

KEYWORDS: *small molecule, bulk heterojunction, additive, organic field effect transistor, polarity, X-ray photoelectron microscopy*

INTRODUCTION

Solution-processable small molecules have recently arisen as promising materials in optoelectronic devices because their intrinsic advantages such as monodispersity, good crystallinity, well-defined chemical structures, and easy purification by column chromatography; problems typically associated with conjugated polymers.[1−4] Recently, bipolar organic field-effect transistors (OFET) have been investigated for use in complementary logic circuits like inverters. These devices are able to greatly simplify logic circuit design, as this device can work for both positive and negative gate biases without the need to separately fabricate transistors based on p- and n-type materials.[3,5] However, it is difficult to fabricate bipolar OFETs using single molecules since organic semiconductors typically exhibit either high electron mobility or high hole mobility, but rarely both.[6,7] To overcome this lack of materials, we have employed bilayer device architectures via subsequent deposition of p- and n-type materials. Bipolar OFETs have been successfully demonstrated based on this principle via coevaporation of p- and n-type small molecules;[8] however, it is challenging to deposit such bilayer FETs via low-cost solution processing techniques, as the active organic semiconductors tend to have similar solubility and cannot be solution coated atop one another. To meet this demand for cost-effective and easily fabricated ambipoler OFETs, bulk heterojunction (BHJ) OFETs comprising solution-processed blends of p/n-type organic semiconductors have great potential as a device fabrication strategy.[9]

Although BHJ OFETs provide an effective strategy for ambipolar device fabrication, poor self-assembly in films of small molecules prepared via solution processing is a major challenge for achieving high-performance devices, because the surface and interface morphologies of the active layer in a device play a critical role affecting the device performance.[10−12] A great number of processing methods for achieving desirable morphology have been demonstrated by means of choice of solvent, post-treatments such as thermal[13] or solvent annealing,[14] processing solvent additives,[15−18] and film forming methods.[19−24] In particular, the use of small amounts of solvent additives in the blend solution has emerged as a powerful technique to control morphologies in organic BHJ OFET, which has been widely used for BHJ solar cells. Among these treatments, processing additive shows promise in studying the correlation between nanomorphology and charge transport behaviors in the BHJ OFET thin film devices geometry. For example, in poly(3-hexylthiophene) (P3HT):fullerene blends, an increase in the hole mobility by 2 orders of magnitude was demonstrated as measured in the BHJ OFETs upon incorporation of small quantities of 1-octanethiol in toluene as a result of changes in the BHJ morphology.[21,25] Heeger and co-workers recently reported changes in field effect carrier mobilities with balanced hole and electron mobilities in the BHJ OFET device, which was consistent with the changes in nanomorphology induced by the use of the CN additive.[26] Even though a number of studies have demonstrated the influence of processing additives on polymer:fullerene BHJ compositions, few studies have addressed the impact of additives in small-molecule-based BHJs so far.

Previously, small-molecule-based BHJ solar cells consisting of a novel donor−acceptor type small molecule (**DTTDPP**) and

Received: February 8, 2013
Accepted: May 23, 2013
Published: May 23, 2013

   dx.doi.org/10.1021/am400546x | ACS Appl. Mater. Interfaces 2013, 5, 4575−4580

Scheme 1. (a) Molecular Structures Used for Active Layer Components and (b) a Test Device Structure

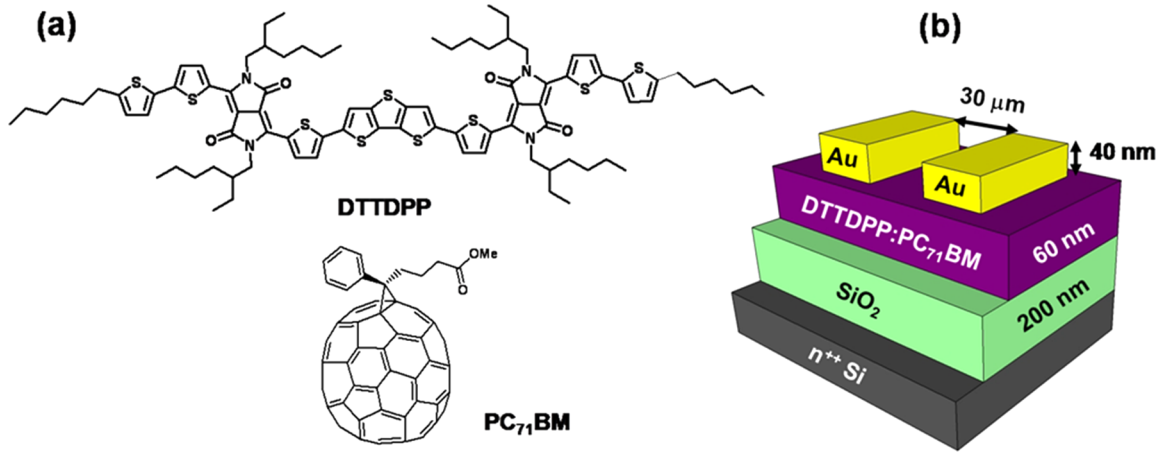

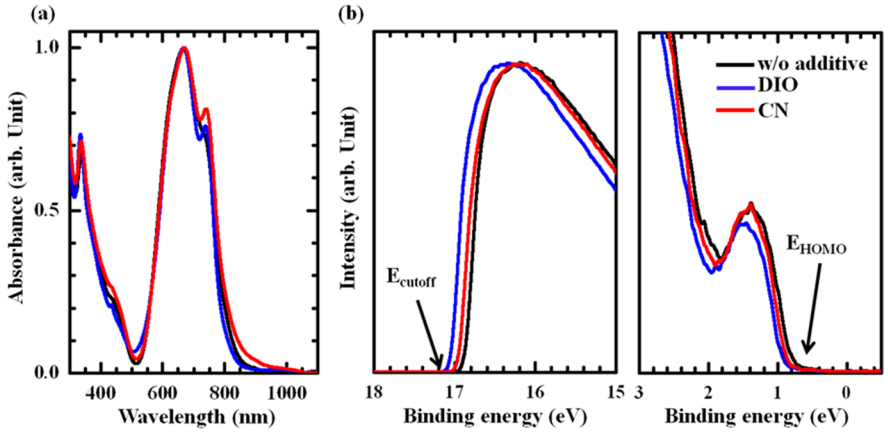

Figure 1. (a) UV−vis spectra for **DTTDPP**:$PC_{71}BM$ blend films without additives (black) and processed with DIO (blue) and CN (red). (b) UPS profiles of the blend films: High binding energy cutoff region (left) and HOMO region (right).

[6,6]-phenyl C_{71} butyric acid methyl ester ($PC_{71}BM$) were introduced and it was found that the device performance could be improved via the addition of solvent additives such as 1,8-diiodooctane (DIO) and 1-chloronaphthalene (CN).[27] Although atomic-force microscopy (AFM) images revealed dramatic changes in morphology, at that time we lacked insight into the possible mechanism of film formation as a function of processing additives. In addition, a universal correlation between molecular structure, processing, film morphology, and device performance in small molecule BHJ systems has not yet been established.

In this contribution, we demonstrate how the processing additives DIO and CN modify electronic properties, charge transport behavior and the molecular self-assembly of small-molecule-based BHJ films. We employ a variety of complementary techniques to investigate a comprehensive range of film properties including ultraviolet photoelectron spectroscopy (UPS) to determine surface electronic structures, OFETs to investigate charge transport properties at the dielectric interface, and X-ray photoelectron microscopy (XPM) to provide insight into the distribution of elements. No change of electronic structures of each component in the BHJ layer was observed by UPS. However, we found that DIO dramatically alters the polarity of the OFET devices from p-type to n-type, whereas the introduction of CN results in balanced bipolar characteristics. XPM was employed to gain further insight into the spatial distribution of each separated phase and the XPM results showed marked changes in the phase separation of each component depending on the choice of additive. These findings provide new insights into the effect of solvent additives on the morphology and performance of small-molecule-based BHJ devices.

The molecular structures of **DTTDPP** and $PC_{71}BM$ and a test device structure are shown in Scheme 1. Figure 1a shows the UV−vis absorption profiles of **DTTDPP**:$PC_{71}BM$ films spin-cast on glass substrates from the neat chloroform and using the same solvents with 1% (v/v) DIO or CN. The absorption peaks at 350 and at 650 nm are due to the contribution of $PC_{71}BM$ and **DTTDPP**, respectively. The solvent additives do not dramatically change the absorption spectrum of the blend with the exception of a small local maximum at ∼750 nm. The absorption band at ∼750 nm in the blend films is visible as a shoulder in the spectrum of the pristine film, which appears as a small peak with DIO and a more pronounced peak with CN. Such an increase in absorption intensity for the low-energy 750 nm band is consistent with absorption because of an aggregated phase, which can be attributed to stronger intermolecular contacts between chromophore units and a more ordered **DTTDPP** phase promoted by processing with DIO and CN.[15,20,28] A similar tendency is observed with the pristine **DTTDPP** absorption profiles under the same conditions (see the

dx.doi.org/10.1021/am400546x | ACS Appl. Mater. Interfaces 2013, 5, 4575−4580

Table 1. Summary of Electronic Properties and Device Characterization of DTTDPP, $PC_{71}BM$, and DTTDPP:$PC_{71}BM$

	additive	E_g (eV)	HOMO (eV)	LUMO (eV)	μ_h ($cm^2/(V\ s)$)	μ_e ($cm^2/(V\ s)$)	V_{th} (V)	I_{on}/I_{off}
DTTDPP	none	1.50	5.07	3.57	8.6×10^{-5}		−4.9	1.8×10^5
	DIO	1.54	5.07	3.53	1.5×10^{-5}		−2.5	1.7×10^4
	CN	1.54	5.06	3.56	5.3×10^{-4}		−1.1	8.7×10^5
$PC_{71}BM$	none	1.70	5.88	4.18		1.0×10^{-3}		
	DIO		5.92	4.22		[a]		
	CN		5.90	4.20		[a]		
BHJ	none	1.52	5.12	3.60	4.0×10^{-5}	1.7×10^{-5}		
	DIO	1.54	5.08	3.52		2.2×10^{-4}		
	CN	1.53	5.12	3.59	2.3×10^{-5}	3.1×10^{-4}		

[a]Dewetting on glass and SiO_2 substrates.

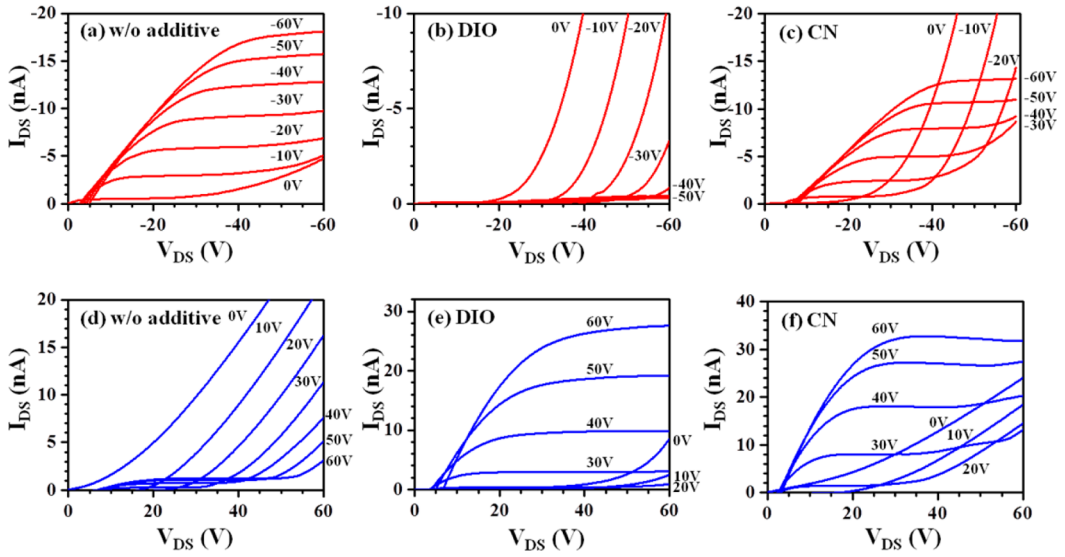

Figure 2. Output characteristics of **DTTDPP**:$PC_{71}BM$ FET devices without and with 1% (v/v) DIO and CN at various gate bias (V_G) and source-drain bias (V_{DS}) from 0 V to ±60 V.

Supporting Information, Figure S1). The optical energy gaps (E_g) in solid states were extracted by linear extrapolation of the long wavelength edge of the spectrum. The E_g values are found to be nearly identical, with values of 1.5 eV for all films regardless of the presence of additives.

To investigate the effect of additives on the energy levels of the blend and each molecule, we carried out ultraviolet photoelectron spectroscopy (UPS) measurements. All thin films were prepared on gold substrates using the same conditions used to prepare films for UV−vis measurement. Figure 1b shows the occupied states of the blend films with and without additives (see the Supporting Information, Figure S2, for UPS spectra of each molecule). The highest occupied molecular orbital (HOMO) energy levels of the films were determined using eq 1

$$\text{HOMO} = h\nu - (E_{\text{cutoff}} - E_{\text{HOMO}}) \quad (1)$$

where $h\nu$ is the incident photon energy (21.2 eV for He I), E_{cutoff} was determined by the linear extrapolation of secondary electron cutoff of the high-binding-energy side of the UPS spectra (15−18 eV) and E_{HOMO} was an onset of the low-binding-energy side (0−3 eV).[29] The lowest unoccupied molecular orbital (LUMO) levels were estimated using the E_g determined from UV−vis and HOMO values determined by UPS.[30] Table 1 contains a summary of these values as well as results from devices, which will be discussed subsequently. One can see no significant changes for the HOMO and LUMO levels of the **DTTDPP**, $PC_{71}BM$ and their blend films resulting from the use of additives. Thus, processing additives such as DIO and CN do not affect the electronic structures of each component and the blend film. To our knowledge, no investigation of the energetic levels of the organic semiconductor films processed from additives by UPS has yet been published.

The impact of the processing additives (DIO and CN) on the charge transporting characteristics of **DTTDPP**:$PC_{71}BM$ BHJ layer were probed using FET devices. Figure 2 shows typical output characteristics of the **DTTDPP**:$PC_{71}BM$ devices without and with additives at various gate bias (V_G) and source-drain voltage (V_{DS}). All device characteristic variables are summarized in Table 1 and the transfer characteristics are displayed in the Supporting Information (Figure S3). The average FET mobility of each transistor was calculated in the saturation regime (V_{DS} = −60 V) by plotting the square root of the drain current versus the gate voltage and fitting the data. A typical p-type dominant transistor behavior is observed at negative V_G for BHJ devices without additives (Figure 2a) which exhibit a hole mobility (μ_h) of 4.0×10^{-5} $cm^2/(V\ s)$. The electron current does not saturate when sweeping V_{DS} from 0 to 60 V at various positive V_G. Surprisingly, the BHJ FETs processed from 1% DIO exhibit n-type transport behavior with an electron mobility (μ_e) of 2.2×10^{-4} $cm^2/(V\ s)$, showing unsaturated hole current regimes under negative bias of V_G and V_{DS} as presented in panels b and e in Figure 2.

Hole transport properties of pristine **DTTDPP** FETs were also examined with the introduction of DIO and CN (Figure 3). The source-drain current (I_{DS}) decreased with DIO, indicating that the DIO is not an effective additive for **DTTDPP**. In contrast, adding a small amount of CN improved the I_{DS} of the pristine **DTTDPP** FET, resulting in a 3.5 times enhancement in μ_h to 5.3 × 10^{-4} $cm^2/(V\ s)$. Meanwhile, analogous measurements of electron transport for pristine $PC_{71}BM$ were attempted, however, dewetting of the $PC_{71}BM$ films on the SiO_2 surface prevented the completion of functioning FET devices. Although surface passivation might resolve the dewetting issue,[31] the comparison with other device configurations would not be valid. Interestingly, bipolar transport behavior is achieved using CN, where the **DTTDPP**:$PC_{71}BM$ FET device has μ_e = 3.1 × 10^{-4} $cm^2/(V\ s)$ and μ_h = 2.3 × 10^{-5} $cm^2/(V\ s)$ (Figure 2c, f). In general, charge transport in a bottom gate and top contact FET takes place primarily within the few nanometers of an active layer at the dielectric/active layer interface, since the charge carriers accumulate at the active/dielectric interface when a gate bias is applied.[32,33] Therefore, the results imply that the interface morphology of the BHJ layers in FETs has been significantly changed with processing additives.

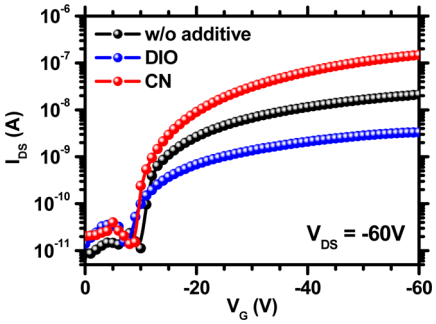

Figure 3. Transfer characteristics at V_{DS} = −60 V without additives (black) and processed with DIO (blue) and CN (red).

X-ray photoelectron microscopy (XPM) measurements of the **DTTDPP**:$PC_{71}BM$ BHJ films were performed in order to map differences in the phase distribution of each component upon adding DIO or CN. XPM images are most informative when used in combination with the chemical information obtained from photoelectron spectra and offer the potential of correlating microscale chemistry and macro-scale material properties.[34,35] In the preliminary analysis, large-area survey spectra were acquired, from which one can obtain qualitative and quantitative information. The spectra exhibit weak Si emission features from all samples, which confirms that photoelectron elemental and chemical images can be provided insight of heterogeneity and phase separation phenomena at the active/dielectric layers. Specific emphasis was made on probing S element distribution against C element, which correlates to the ratio of **DTTDPP** to $PC_{71}BM$. Figure 4 shows XPM images of the blend films with and without additives for the S 2p intensity distribution normalized by the C 1s intensity displaying two distinct domains (red and blue). The red phase corresponds to a greater concentration of **DTTDPP** phase, whereas the blue phase is assigned to an increased concentration of $PC_{71}BM$. The blend film prepared from pristine chloroform (Figure 4a) exhibits a small portion of **DTTDPP** domains relative to $PC_{71}BM$ domains. The blend film processed from DIO (Figure 4b) shows that $PC_{71}BM$ is dominant on the surface without significant S 2p signal. In contrast, evenly distributed phases of each component in the blend film processed with CN were observed. In addition, the topographic study of the **DTTDPP**:$PC_{71}BM$ BHJ films prepared from pure chloroform showed uneven and spherical features with average diameters of 200 nm.[27] A rougher surface morphology was developed by adding DIO, while a smoother and more desirable phase-separated morphology was achieved with CN. With the corresponding XPM mapping, it can be inferred that the spherical features and the rough surface morphology observed from AFM images are mainly formed by $PC_{71}BM$ aggregation.

Figure 5 presents schematic illustrations of the **DTTDPP**:$PC_{71}BM$ internal morphologies based on the OFET, AFM and XPM analyses. Green and purple illustrate pure **DTTDPP** and $PC_{71}BM$, respectively. DIO leads to the aggregation of **DTTDPP** embedded in a $PC_{71}BM$ matrix and the blend film with CN forms an interpenetrating network of each component. The p-type transistor behavior of devices without additives implies an enrichment layer of **DTTDPP** at the dielectric interface supported by partially red features observed in XPM (Figure 4a) and aggregated $PC_{71}BM$ clusters at the surface of the AFM images, as shown in Figure 5a. In contrast, the BHJ film processed with DIO exhibits $PC_{71}BM$ dominant phase distribution in XPM images, n-type charge transport behavior and large aggregation in AFM surface images; these observations would be consistent with aggregated **DTTDPP** domains being surrounded by a continuous $PC_{71}BM$ phase, leading to disconnected hole transport (Figure 5b). The bipolar properties of the devices processed from CN suggest well-separated phase distribution and bicontinuous, percolated networks at the dielectric interface (Figure 5c).

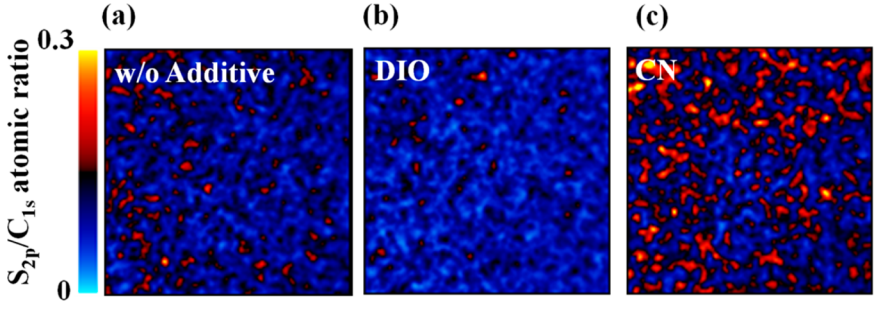

Figure 4. XPM images (size: 100 μm × 100 μm) of **DTTDPP**:$PC_{71}BM$ blend films (a) without additive and with (b) DIO and (c) CN. (Red represents the **DTTDPP**, whereas blue represents the $PC_{71}BM$.).

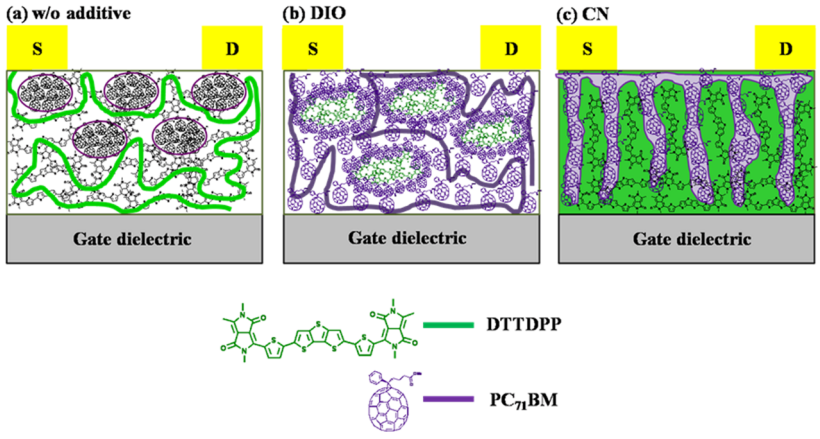

Figure 5. Schematic illustrations of proposed donor/acceptor distribution in OFET devices.

We next consider the causes of differences in phase separation and how these differences relate to the solubility of each component and the rate of solvent evaporation. When films are fabricated from neat chloroform, $PC_{71}BM$ shows a relatively greater tendency to self-assemble and form poly crystalline domains during to the fast evaporation of the solvent, while **DTTDPP** is not able to completely self-assemble during the short time period it takes for the chloroform to evaporate. The pristine **DTTDPP** FET with DIO shows poor p-type device performance, indicating that although DIO may slow the evaporation rate of the solvent and provide more time for self-assembly, it is a poor additive for **DTTDPP** and does not promote desirable self-assembly in this material. Meanwhile, $PC_{71}BM$ films processed with DIO show improvement, as previously reported.[36] Accordingly, during film formation in the BHJ using DIO as an additive, $PC_{71}BM$ is well distributed from the dielectric interface to the top, whereas **DTTDPP** aggregates poorly during the slow evaporation of DIO. As proven in **DTTDPP** FET devices and as observed in the literature, CN is an effective additive for both **DTTDPP** and $PC_{71}BM$, promoting desirable self-assembly and distribution of each material throughout BHJ layer; leading to balanced carrier transport.[27]

In summary, we report on the influence of the solvent additives DIO and CN on the energy levels, charge transport properties and phase distribution of the **DTTDPP**:$PC_{71}BM$ BHJ system. The polarities of BHJ FET devices without additives and with DIO and CN are p-type, n-type and bipolar, respectively, regardless of their energetic levels of the **DTTDPP**, $PC_{71}BM$ and their blend. The polarity of the devices was determined by the phase distribution of each component, which was controlled via processing additives. Compared to the pristine blend film, the use of DIO led to film properties consistent with **DTTDPP** aggregation within a continuous $PC_{71}BM$ phase, whereas the introduction of CN gives rise to the even distribution of donor/acceptor phases on the dielectric/active layer interface. It is confirmed that desirable, interpenetrated phase separation behavior is achieved with CN additive by XPM analysis together with the corresponding OFET characteristics. Our findings indicate that (i) additives do not affect the HOMO/LUMO levels of **DTTDPP**, $PC_{71}BM$ or blends of the two materials, (ii) a proper selection of additives can lead to efficient charge transport, and (iii) the use of additives critically influences the film morphology and mixing of donor/acceptor materials, allowing significant improvements in device performance.

EXPERIMENTAL SECTION

UV–Vis Absorption Measurement. Solutions of 5 mg/mL **DTTDPP**, as well as 5 mg/mL **DTTDPP** with 1% v/v DIO or CN were prepared in chloroform. In addition, blend solutions of **DTTDPP**:$PC_{71}BM$ (1:1 w/v) in chloroform with concentration of 14 mg/mL were prepared without or with 1% v/v DIO or CN. Thin films were prepared by spin-casting from each solution onto a glass substrate at 2000 rpm for 40 s. Absorption spectra were measured with a Beckman Coulter DU 800 series UV–vis spectrophotometer.

UPS Measurement. 75 nm thick gold films were deposited on precleaned Si substrates with a thin native oxide. The same solutions used for to collect absorption spectra were spin-cast onto gold films using the same conditions. Film fabrication was done in a N_2-atmosphere glovebox. To minimize the possible influence of exposure to air, we then transferred the films from the N_2-atmosphere drybox to the analysis chamber inside an air-free sample holder. Subsequently, the samples were kept inside a high-vacuum chamber overnight. The UPS analysis chamber was equipped with a hemispherical electron-energy analyzer (Kratos Ultra Spectrometer) and was maintained at a pressure of 1.0×10^{-9} Torr. UPS measurements were carried out using a He I ($h\nu$ = 21.2 eV) light source. During UPS measurements, a sample bias of −9 V was used in order to separate the sample and the secondary edge for the analyzer.

FET Fabrication and Characterization. All OFETs were fabricated on heavily n-type doped Si wafers with a 200 nm thick thermally grown SiO_2 layer. The n-type doped Si substrate functioned as the gate electrode and the SiO_2 layer functioned as the gate dielectric. Solutions mentioned above were spin-cast at a spin speed of 2000 rpm for 40 s. The film thickness was approximately 60 nm. All deposition was carried out in N_2-glovebox. Forty-nanometer-thick Au electrodes were deposited by thermal evaporation using a shadow mask. Channel length (L) and channel width (W) were 30 μm and 1 mm, respectively. Electrical characterization was performed under a N_2 atmosphere using a Keithley 4200 semiconductor parametric analyzer.

XPS/XPM Measurement. Sample preparation was identical to the procedure used for UPS measurements. The XPS analysis chamber was equipped with a hemispherical electron-energy analyzer (Kratos Ultra Spectrometer) and was maintained at 1.0×10^{-9} Torr. The XPS was measured using monochromatized Al Kα ($h\nu$ = 1486.6 eV) excitation. The electron energy analyzer was operated at constant pass energy of 80 eV for mapping experiment and 20 eV for high-resolution acquisition, respectively. The S 2p, O 1s, N 1s, and C 1s photoelectron images were employed at a small magnification of 100 μm × 100 μm and an acquisition time of 5–10 min per image. The image-to-spectra measurement were acquired in a series of 26 images over the binding energy range 280–290 eV for C 1s, 160–170 eV for S 2p, and 395–405 eV for N 1s, respectively, and 38 images over the binding energy

dx.doi.org/10.1021/am400546x | ACS Appl. Mater. Interfaces 2013, 5, 4575–4580

range 525−540 eV for O 1s with a 0.4 eV step. Images were converted to spectra for multivariate image analysis using CASAXPS software (Ver. 2.3.12).

■ ASSOCIATED CONTENT

Ⓢ Supporting Information

UV−vis absorption spectra, UPS profiles, and additional device information of transfer characteristics and output characteristics for BHJ FETs and each pristine material. This material is available free of charge via the Internet at http://pubs.acs.org.

■ AUTHOR INFORMATION

Corresponding Author

*E-mail: brightium@unist.ac.kr (B.W.); seojh@dau.ac.kr (J.H.S.).

Notes

The authors declare no competing financial interest.

■ ACKNOWLEDGMENTS

This work was supported by the Dong-A University research fund. We gratefully thank Prof. G. C. Bazan and Prof. A. J. Heeger (University of California Santa Barbara) for their fruitful help and the use of their facilities.

■ REFERENCES

(1) Coropceanu, V.; Cornil, J.; da Silva Filho, D. A.; Olivier, Y.; Silbey, R.; Brédas, J.-L. *Chem. Rev.* **2007**, *107*, 926−952.
(2) Walker, B.; Kim, C.; Nguyen, T.-Q. *Chem. Mater.* **2011**, *23*, 470−482.
(3) Liu, Y.-Y.; Song, C.-L.; Zeng, W.-J.; Zhou, K.-G.; Shi, Z.-F.; Ma, C.-B.; Yang, F.; Zhang, H.-L.; Gong, X. *J. Am. Chem. Soc.* **2010**, *132*, 16349−16351.
(4) Fan, H.; Shang, H.; Li, Y.; Zhan, X. *Appl. Phys. Lett.* **2010**, *97*, 133302.
(5) Singh, Th. B.; Günes, S.; Marjanović, N.; Sariciftci, N. S.; Menon, R. *J. Appl. Phys.* **2005**, *97*, 114508.
(6) Tang, M. L.; Reichardt, A. D.; Miyaki, N.; Stoltenberg, R. M.; Bao, Z. *J. Am. Chem. Soc.* **2008**, *130*, 6064−6065.
(7) Tang, M. L.; Oh, J. H.; Reichardt, A. D.; Bao, Z. *J. Am. Chem. Soc.* **2009**, *131*, 3733−3740.
(8) Meijer, E. J.; de Leeuw, D. M.; Setayesh, S.; van Veenendaal, E.; Huisman, B.-H.; Blom, P. W. M.; Hummelen, J. C.; Scherf, U.; Klapwijk, T. M. *Nat. Mater.* **2003**, *2*, 678−682.
(9) Zaumseil, J.; Sirringhaus, H. *Chem. Rev.* **2007**, *107*, 1296−1323.
(10) Walker, B.; Tamayo, A. B.; Dang, X.-D.; Zalar, P.; Seo, J. H.; Garcia, A.; Tantiwiwat, M.; Nguyen, T.-Q. *Adv. Funct. Mater.* **2009**, *19*, 3063−3069.
(11) Sirringhaus, H. *Adv. Mater.* **2005**, *17*, 2411−2425.
(12) Brédas, J. L.; Calbert, J. P.; da Silva Filho, D. A.; Cornil, J. *Proc. Natl. Acad. Sci. U. S.A.* **2002**, *99*, 5804−5809.
(13) Walker, B.; Tamayo, A.; Duong, D. T.; Dang, X.-D.; Kim, C.; Granstrom, J.; Nguyen, T.-Q. *Adv. Energy Mater.* **2011**, *1*, 221−229.
(14) Wei, G.; Lunt, R. R.; Sun, K.; Wang, S.; Thompson, M. E.; Forrest, S. R. *Nano Lett.* **2010**, *10*, 3555−3559.
(15) Lloyd, M. T.; Mayer, A. C.; Subramanian, S.; Mourey, D. A.; Herman, D. J.; Bapat, A. V.; Anthony, J. E.; Malliaras, G. G. *J. Am. Chem. Soc.* **2007**, *129*, 9144−9149.
(16) Moet, D. J. D.; Lenes, M.; Morana, M.; Azimi, H.; Brabec, C. J.; Blom, P. W. M. *Appl. Phys. Lett.* **2010**, *96*, 213506.
(17) Walker, B.; Liu, J.; Kim, C.; Welch, G. C.; Park, J. K.; Lin, J.; Zalar, P.; Proctor, C. M.; Seo, J. H.; Bazan, G. C.; Nguyen, T.-Q. *Energy Environ. Sci.* **2013**, *6*, 952−962.
(18) Cho, S.; Lee, J. K.; Moon, J. S.; Yuen, J.; Lee, K.; Heeger, A. J. *Org. Electron.* **2008**, *9*, 1107−1113.
(19) Kwon, S.; Park, J. K.; Kim, G.; Kon, J.; Bazan, G. C.; Lee, K. *Adv. Energy Mater.* **2012**, *2*, 1420−1424.
(20) Gaynor, W.; Lee, J.-Y.; Peumans, P. *ACS Nano* **2010**, *4*, 30−34.
(21) Peet, J.; Kim, J. Y.; Coates, N. E.; Ma, W. L.; Moses, D.; Heeger, A. J.; Bazan, G. C. *Nat. Mater.* **2007**, *6*, 497−500.
(22) Hoven, C. V.; Dang, X. D.; Coffin, R. C.; Peet, J.; Nguyen, T.-Q.; Bazan, G. C. *Adv. Mater.* **2010**, *22*, E63−E66.
(23) Su, M.-S.; Kuo, C.-Y.; Yuan, M.-C.; Jeng, U.-S.; Su, C.-J.; Wei, K.-H. *Adv. Mater.* **2011**, *23*, 3315−3319.
(24) Xin, H.; Guo, X.; Ren, G.; Watson, M. D.; Jenekhe, S. A. *Adv. Energy Mater.* **2012**, *2*, 575−582.
(25) Cho, S.; Yuen, J.; Kim, J. Y.; Lee, K.; Heeger, A. J. *Appl. Phys. Lett.* **2006**, *89*, 153505.
(26) Moon, J. S.; Takacs, C. J.; Cho, S.; Coffin, R. C.; Kim, H.; Bazan, G. C.; Heeger, A. J. *Nano Lett.* **2010**, *10*, 4005−4008.
(27) Park, J. K.; Kim, C.; Walker, B.; Nguyen, T.-Q.; Seo, J. H. *RSC Adv.* **2012**, *2*, 2232−2234.
(28) Loser, S.; Bruns, C. J.; Miyauchi, H.; Ortiz, R. P.; Facchetti, A.; Stupp, S. I.; Marks, T. J. *J. Am. Chem. Soc.* **2011**, *133*, 8142−8145.
(29) Seo, J. H.; Nguyen, T.-Q. *J. Am. Chem. Soc.* **2008**, *130*, 10042−10043.
(30) Tengstedt, C.; Osikowicz, W.; Salaneck, W. R.; Parker, I. D.; Hsu, C.-H.; Fahlman, M. *Appl. Phys. Lett.* **2006**, *88*, 53502.
(31) Jasieniak, J. J.; Hsu, B. B. Y.; Takacs, C. J.; Welch, G. C.; Bazan, G. C.; Moses, D.; Heeger, A. J. *ACS Nano* **2012**, *6*, 8735−8745.
(32) Dinelli, F.; Murgia, M.; Levy, P.; Cavallini, M.; Biscarini, F.; de Leeuw, D. M. *Phys. Rev. Lett.* **2004**, *92*, 116802.
(33) Kobayashi, S.; Nishikawa, T.; Takenobu, T.; Mori, S.; Shimoda, T.; Mitani, T.; Shimotani, H.; Yoshimoto, N.; Ogawa, S.; Iwasa, Y. *Nat. Mater.* **2004**, *3*, 317−322.
(34) Vohrer, U.; Blomfield, C.; Page, S.; Roberts, A. *Appl. Surf. Sci.* **2005**, *252*, 61−65.
(35) Artyushkova, K.; Fulghum, J. E. *Surf. Interface Anal.* **2001**, *31*, 352−361.
(36) Lou, S. J.; Szarko, J. M.; Xu, T.; Yu, L.; Marks, T. J.; Chen, L. X. *J. Am. Chem. Soc.* **2011**, *133*, 20661−20663.